Effect of a Zinc Interlayer on a Cu/Al Lap Joint in Ultrasound-Assisted Friction Stir Welding

Shujin Chen, Di Wang, Ruifeng Li, Bin Liu, and Jianxin Wang

This study proposes a welding process, ultrasound-assisted friction stir welding of dissimilar Al/Cu metals. Zinc foil is melted using the heat generated by a pinless stirring tool, and the molten intermediate layer is stirred by ultrasonic cavitation to achieve an effective connection. The metallurgical reaction behavior of the joint under the action of the sound field was studied, and the effects of different microstructures on the joint performance were analyzed. Specifically, the following observations were reported in this study: (1) When ultrasound assistance was used, the cavitation effect changed the brittle intermetallic compounds of Al_2Cu from a continuous distribution to a block distribution, and the mechanical properties of the joint were greatly improved; (2) the effects of the thickness of the zinc were also determined. The results showed that the highest shear tensile force was obtained when the thickness of the zinc foil was 0.2 mm. When the thickness was 0.3 mm, the ultrasound effect was weakened. The copper-side interface generated a zigzag-shaped $Al_{4.2}Cu_{3.2}Zn_{0.7}$ layer with a thickness of 3.4 μm and had a continuous distribution. Increasing the thickness of the zinc to 0.5 mm, however, drastically decreased the mechanical properties of the joint due to incomplete melting of the zinc layer.

1. Introduction

Cu alloys have been widely applied in the manufacturing of air conditioners, refrigerators, wireways, and central processing unit (CPU) radiators. However, the high price and density of Cu have limited its applications. Therefore, the joining of Al to Cu has been used to meet the increasing demand for Cu since this method not only combines the advantages of high thermal and electrical conductivity but also lowers the price (Ref 1-3). However, joining dissimilar Cu and Al metals is a significant challenge because of the poor weldability that arises from their different chemical, mechanical, and thermal properties and the formation of brittle Cu-Al intermetallic compounds (IMCs) (Ref 4, 5). Conventional fusion welding methods have high work temperatures that exceed the melting temperature of the base metal. Thus, these methods are not recommended because they lead to further solidification defects that are unsafe for the application of welded structures.

Solid-phase connection technologies, such as friction stir welding (FSW) and ultrasonic welding, have been widely applied in recent years due to their particular advantages and provide new directions for the preparation and development of Al-Cu structures. However, IMCs have also been found in friction stir welded Al-Cu joints when the new welding method

is used to join dissimilar metal materials (Ref 6-8). For example, Jiahu Ouyang et al. (Ref 9) reported that the IMCs of Al_2Cu, $AlCu$ and Al_4Cu_9 appeared in an FSW butt joint of 6061 aluminum alloy and pure copper.

To avoid the formation of brittle IMCs in the production of high-strength joints, previous investigations of dissimilar metal joining used an interlayer (Ref 10). For example, J. P. Oliveira et al. (Ref 11) joined NiTi and Ti_6Al_4V using a niobium interlayer and no brittle intermetallic compounds were observed. Thus, the selection of an appropriate interlayer could be successfully applied to join Al and Cu. Zn was chosen because of its ability to interact well with both Al and Cu at high temperatures, as seen in the Al-Zn (Ref 12) and Cu-Zn (Ref 13) binary phase diagrams. For example, Elrefaey et al. (Ref 14) used Zn foil as an intermediate layer to join Al and Cu by FSW, which not only inhibited the formation of brittle compounds but also expanded their distribution range.

Nevertheless, by adding an interlayer in the middle of the Al/Cu joint, the production of aluminum-copper IMCs can be inhibited, and the mechanical properties of the joint can be improved. However, the need for a pin in FSW results in an aesthetically undesirable keyhole and groove (channel) which significantly influence the weld strength. Zhang et al. (Ref 15) reported that the same effect can be achieved by using a pinless tool for welding. However, because friction exists between the stirring tool and the upper plate, the Zn layer cannot be stirred. As a result, the composition of the weld zone is not uniform, which causes the aluminum and copper elements to aggregate easily and form a brittle IMC at the intermediate layer.

Ultrasound welding provides a new approach. Ultrasound-assisted brazing, another environmentally friendly welding method, is also widely used in the joining of dissimilar metals. In previous studies (Ref 16, 17), when using this method to braze joints, the ultrasound wave propagating to the liquid-phase brazing seam can create a cavitation effect and an acoustic flow effect near the solid–liquid interface of the joints. These effects promote the wetting and spreading of the liquid

Shujin Chen, Di Wang, Ruifeng Li, Bin Liu, and **Jianxin Wang,** National Demonstration Center for Experimental Materials Science and Engineering Education, Jiangsu University of Science and Technology, Zhenjiang 212003, China. Contact e-mail: wangdi769@foxmail.com.

solder on the base metal surface and the metallurgical reaction between the solder alloy and the base metal and effectively refine the solidified structure of the metal, improving the homogeneity of the structure. Nevertheless, because the brazing process needs to be carried out on a heating stage or furnace and the equipment requirements are restrictive, the requirements cannot be met for long welds or large-area welding. These problems can be overcome by using pinless FSW with high rotation speed (Ref 18) as the heat and pressure source and ultrasound assistance to stir the interlayer. Few previous studies have explored this approach.

Building on the prior background research described above, this study uses ultrasound-assisted FSW to fabricate Al/Cu heterogeneous metal joints. The microstructures of the joints were optimized by changing the thickness of the interlayer to improve the mechanical properties of the joints. In particular, this study focuses on the interfacial metallurgical reaction behavior of the joint under an acoustic field and the influence of different microstructures on the joint performance.

2. Experimental Procedures

In this study, a pinless tool made of H13 tool steel with shoulder diameters of 10 mm was designed and used. A commercial 1-mm-thick sheet of 6061-T6 Al alloy (composition in wt.%: Al-1Mg-0.62Si-0.5Fe-0.28Cu-0.1Mn-0.05Zn) and a 1-mm-thick sheet of pure copper were selected for joining. Pure zinc foil was used as the filling metal. The sizes of the aluminum plate and the copper plate were 80 mm × 100 mm and 80 mm × 80 mm, respectively. Pure zinc with thicknesses of 0.2 mm, 0.3 mm and 0.5 mm was used as the interlayer, with a size of 90 mm × 20 mm, as shown in Fig. 1.

Prior to the welding experiments, the faying surfaces of the aluminum and the copper were sanded using 800 emery papers. Next, the plates were cleaned with ethanol followed by acetone before joining. The assembly was fastened in an overlapping configuration with the Cu substrate placed under the Al substrate and the zinc foil sandwiched as an interlayer between the Cu and Al substrates, as seen in Fig. 1. For comparison, the FSB process was classified into two groups, with or without ultrasound assistance, with zinc thicknesses of 0.2 mm, 0.3 mm and 0.5 mm in each group. The same parameters (plunge depth of 0.2 mm, travel speed of 100 mm/min, rotation speed of 11,000 rpm and rotation tool tilt angle of 0°) were used. The ultrasound parameters were set to a vibration frequency of 20 kHz and a power of 960 W. The welding parameters are summarized in Table 1. The samples corresponding to the different thicknesses of zinc in Group A are referred to as A0.2, A0.3 and A0.5, while the samples corresponding to the different thicknesses of zinc in Group B are referred to as B0.2, B0.3 and B0.5.

After the experiment was completed, the shear tensile samples (130 mm long and 12.5 mm wide) and metallographic samples (25 mm long, 5 mm wide and 2 mm thick) were obtained by wire cut electrical discharge machining (WEDM). Two tensile samples were taken from each test plate. The metallographic samples were mounted and then mechanically polished with carbide abrasive papers. Finally, the macrostructure was observed using an optical microscope. The morphology of the microstructure was further analyzed by scanning electron microscopy (SEM) with a secondary electron imaging (SEI) model, and the chemical composition of the intermediate layer was determined by an energy-dispersive x-ray (EDS) system. X-ray diffraction (XRD) was used to determine the phase of the fracture surface. Tensile tests were carried out at room temperature with an electronic drawing machine at a drawing rate of 1 mm/min.

3. Results

3.1 Surface Macroscopic Appearance

Figure 2 shows the surface morphology of the weld. All the welding surfaces are similar, so only one representative graph was selected for analysis from the B0.2 sample. As seen from the figure, because the tool tilt angle was set at 0° and the plunge depth was 0.2 mm, a large flash formed at the retreating side of the joint, but none of the joints presented substantial macroscopic defects. In addition, the Zn was melted, and extrusions appeared both at the beginning and at the end of the welding, as shown in the enlarged area in the figure, indicating that the zinc layer melted under these welding conditions. However, this result was not observed in the A0.5 sample, indicating that under these conditions, Zn cannot be completely melted due to insufficient heat production. Thus, the A0.5 sample will not be mentioned below.

3.2 Microscopy Analysis

Table 1 List of the FSB parameters

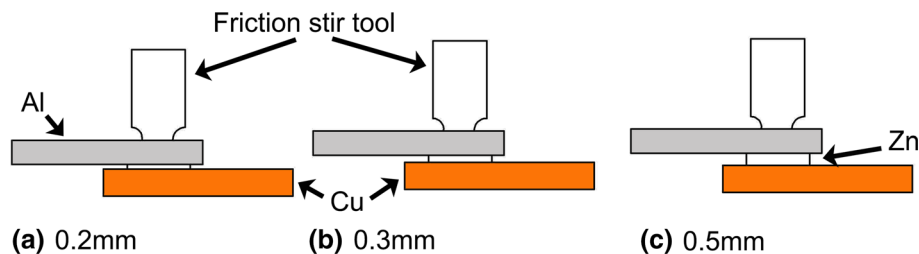|	Group A	Group B
Thickness of zinc, mm	0.2, 0.3, 0.5	0.2, 0.3, 0.5
Ultrasound assistance	No	Yes
Plunge depth, mm	0.2	0.2
Traverse speed, mm/min	100	100
Rotation speed, rpm	11,000	11,000

Fig. 1 Schematic diagram with different zinc layer thicknesses, (a) 0.2 mm, (b) 0.3 mm, (c) 0.5 mm
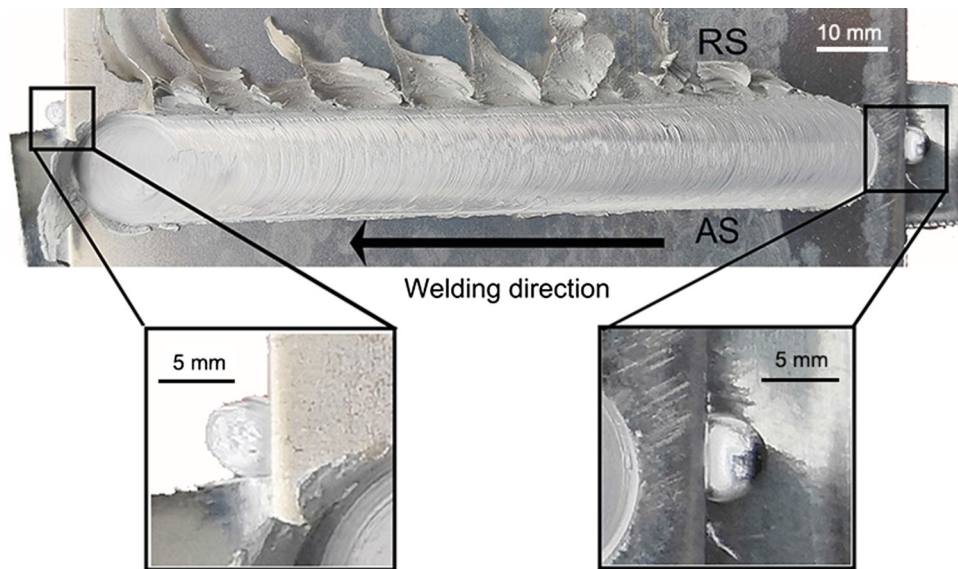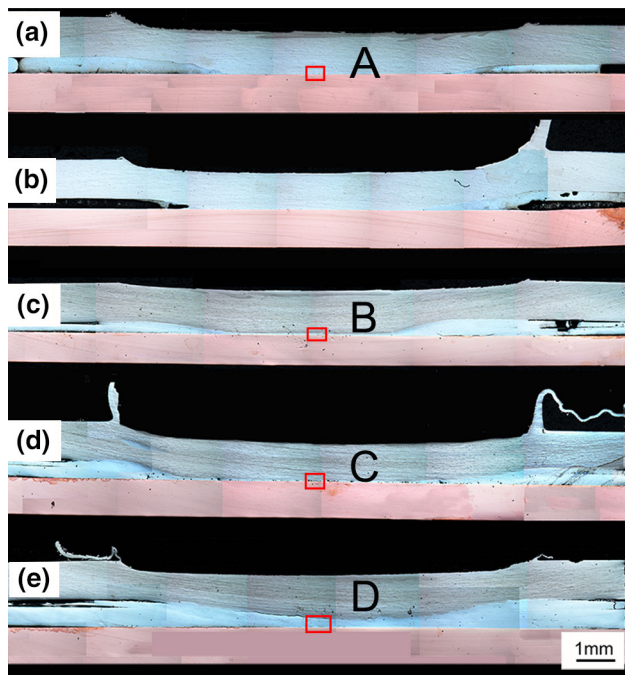
Fig. 2 Typical morphology of the weld surface

Fig. 3 Cross-sectional macrostructures of the joint interface, produced using different parameters. (a) A0.2, (b) A0.3, (c) B0.2, (d) B0.3, and (e) B0.5

3.2.1 Cross-Sectional Macrostructure. Figure 3 shows the intersecting surface morphology of the weld under different process conditions. The 0.2 mm plunge resulted in a weld zone that was significantly concave on the aluminum side. The corresponding interlayer also appeared to have a bowl-like structure, while the middle interlayer was too thin to be observed. These observations indicate that sufficient heat was generated during the welding process to melt the Zn layer, but the thickness of the original zinc layer was still maintained on both sides due to the insufficient heat and pressure. However,

compared to those of the other samples, the intermediate layer of the B0.5 sample was thick, and no voids or cracks appeared. To further analyze the structure of the intermediate layer and the effect of ultrasound on the quality of the weld, SEM and EDS analysis of the interface is required, as shown below.

3.2.2 SEM Analysis of the Cross Sections of the Welds. As shown in Fig. 4, SEM images of the weld area in the interlayer were obtained from the areas indicated by the red rectangles in Fig. 3. Considering that the mechanical properties of the A0.3 and A0.2 samples are similar, which will be demonstrated in Sect. 3.3, only the A0.2 sample was selected for comparative analysis to illustrate the effects of ultrasound on joint quality. Figure 4(a) shows the interface microstructure of A0.2. Combined with EDS, the results show that the interlayer is mainly composed of white bulk $CuZn_5$ and gray eutectic Al-Zn, which are homogeneously distributed in the middle layer. The eutectic Al-Zn layer with a thickness of 1 μm is near the aluminum substrate, while two layers of distinct colors appear near the copper substrate.

Figure 4(b) shows the interface microstructure of B0.2, which was prepared with ultrasound assistance and was completely altered compared with that of the A0.2 sample. The thickness of the interlayer decreased from 43 μm to 28 μm. Additionally, the interlayer structure was still composed of $CuZn_5$ and eutectic Al-Zn, but the amount and morphology had changed. The proportion of $CuZn_5$ decreased and was distributed in the middle of the interlayer, while the proportion of eutectic Al-Zn increased along both sides of the substrate. This result indicates that the aluminum content in the interlayer increased. Notably, a homogeneous bulk section was formed at the copper interface but merely emerged as a lump and did not exhibit a lamellar distribution. The chemical composition (in at.%) of the heterogeneous IMC region was 71.1Al-28.9Cu. Based on the ratio of Al to Cu in the atomic composition given by the EDS results, the bulk section is Al_2Cu. It also worth to be notice that the eutectic structure is very small compared with that shown in Fig. 6(a) and is not distributed in layers. This kind of structure is quite compact and does not fracture easily. It indicates that applying ultrasound during the welding process is beneficial for refining the interlayer structure.
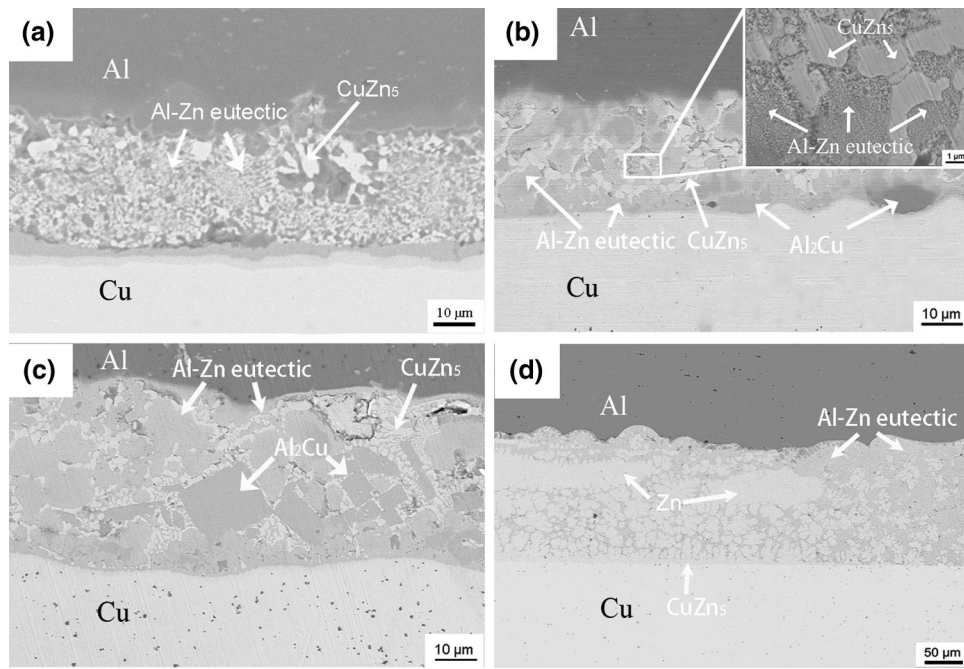
Fig. 4 Cross-sectional SEM micrograph at the center of the different sample. (a) A0.2, (b) B0.2, (c) B03, and (d) B0.5
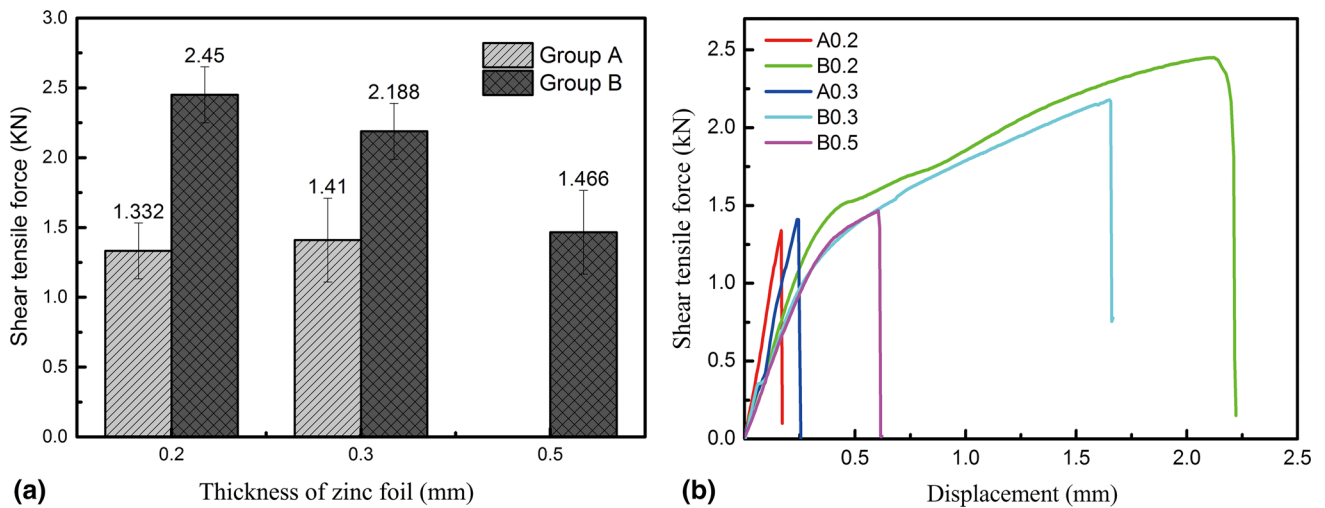

Fig. 5 (a) Dependence of the shear tensile force and (b) typical shear tensile force–displacement curves under different conditions

As the thickness of the zinc foil increased to 0.3 mm, the interface changed again, as shown in Fig. 4(c), and the interfacial thickness increased to 40 μm. In addition to the formation of $CuZn_5$ and eutectic Al-Zn, there were rectangular dark substances in the interface. EDS analysis shows that these substances were Al_2Cu. Because the 0.3 mm zinc foil was used, the increased zinc content led to increased dissolution of the Al into the zinc layer per unit volume, which led to formation of a brittle phase of Al_2Cu in the interlayer. Using flame joining, some researchers (Ref 19, 20) also obtained Al_2Cu in the interfacial layer, which may be attributed to transition corrosion of the Al base metal in the solder layer during welding.

However, further increasing the thickness of the zinc foil to 0.5 mm, as shown in Fig. 4(d), revealed that there was original zinc at the interfacial layer. Compared with the interface morphology under other conditions, the thickness of the interlayer increased significantly to 150 μm. Eutectic Al-Zn can be found along the aluminum substrate, and the Al/Zn interfacial layer exhibits irregularity.

3.3 Mechanical Behavior of the Welded Joint

3.3.1 Lap Shear Tensile Test. Figure 5(a) shows the shear strength of the joints under different parameters. The failure load remains the same and then decreases significantly to 0 kN (the joint broke before being clamped) with increasing
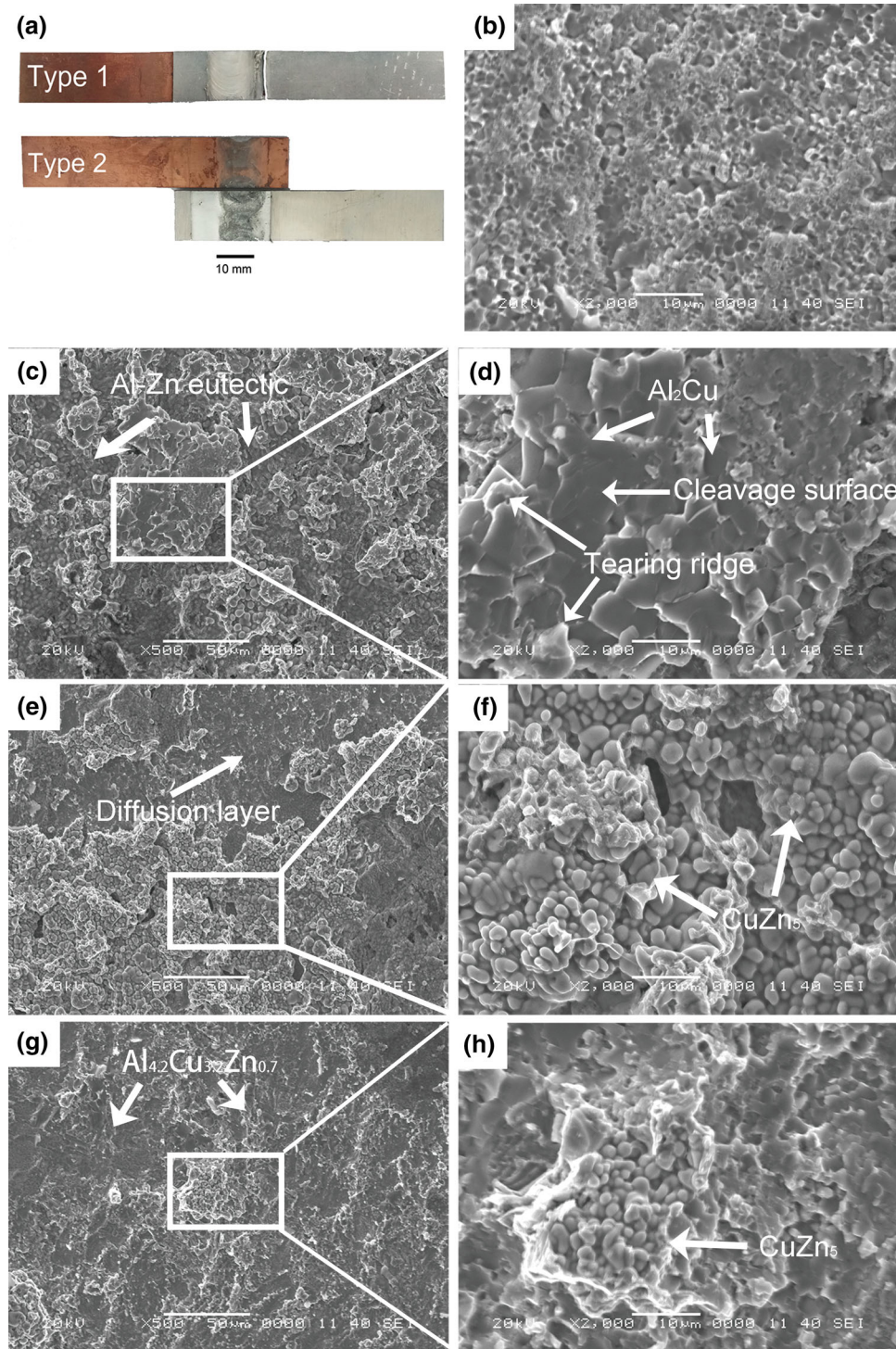
Fig. 6 (a) Two types of fractures (Type 1 is fractured at the aluminum side, and Type 2 is fractured at the interface); (b) SEM image of the aluminum side fracture of the B0.2 sample; (c) and (d) SEM images of the Cu-side fractures of the A0.2 sample; (e) and (f) SEM images of the Cu-side fractures of the B0.2 sample; (g) and (h) SEM images of the Cu-side fractures of the B0.3 sample

zinc foil thickness in Group A, while the failure load decreases with increasing zinc foil thickness in Group B. The highest shear force (2.45 kN) was found in the B0.2 sample, which implies that the FSB process with ultrasound assistance is effective for dissimilar Cu and Al metals with a Zn metal filler. Figure 5(b) shows the typical shear tensile force–displacement curves under different conditions. The

displacement increased when ultrasound was applied, especially for the B0.2 sample, which had the highest displacement.

3.3.2 Fracture Behavior. Two types of fracture modes are shown in Fig. 6(a). Only the B0.2 sample broke in type 1 mode (in the base aluminum metal, not at the interface). The others fractured in type 2 mode (near the copper side). Figure 6(b)
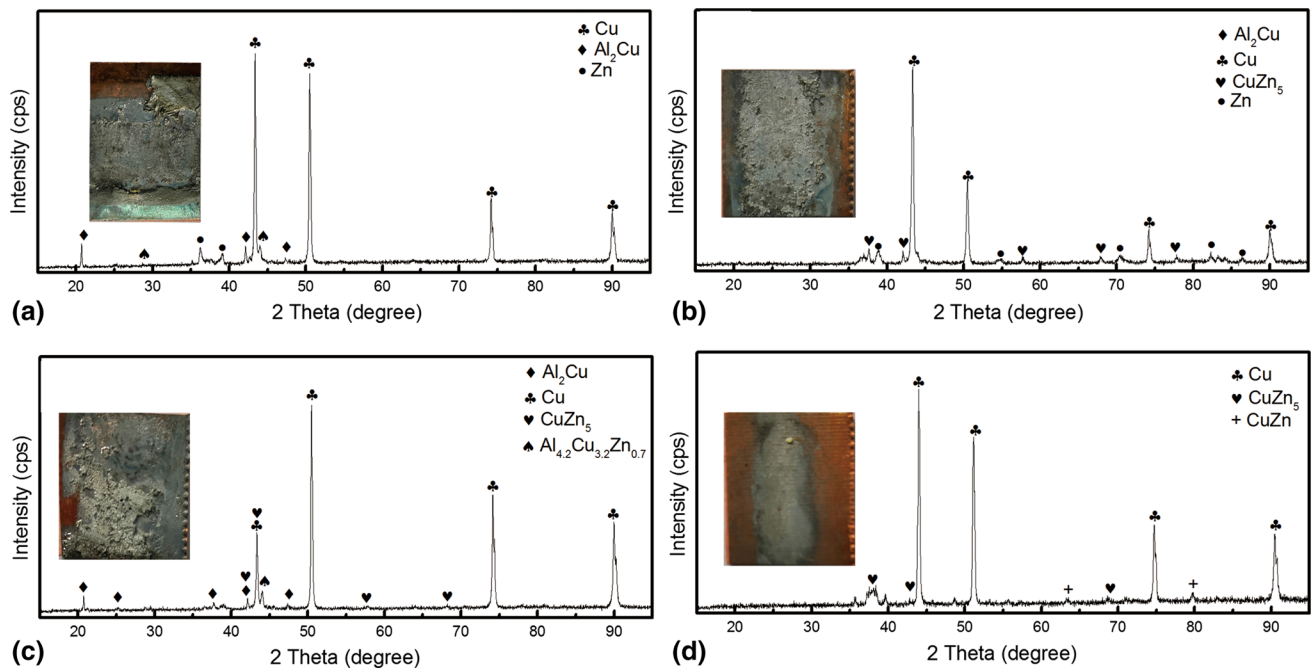
Fig. 7 XRD patterns of the Cu-side fractures under different process conditions. (a) A0.2, (b) B0.2, (c) B0.3, and (d) B0.5

shows the aluminum side of the B0.2 fractured sample. It is interesting that many tiny pits appear on the surface of the aluminum, with diameters of 2-3 μm. This is similar to the "dissolution pit" formed by the ultrasound cavitation mentioned by Chen et al. (Ref 21). No similar morphology was observed on the aluminum surface of the other samples. Thus, the ultrasound effect is most clear in the B0.2 sample.

Figure 6(c), (d), (e), (f), (g), and (h) shows the fractography at the lower Cu plate obtained using SEM. Figure 7 illustrates the intensity peaks of various compounds at 2θ diffraction angles for the Cu side. The fracture of the B0.5 sample is not selected in Fig. 6 because the fracture occurred at the interface between $CuZn_5$ and Cu. Because the B0.2 sample was broken at the Al substrate, the sample was exposed to a low temperature for 30 min to make it brittle and then detached with a hammer to expose the weld nugget in the Cu metal.

Figure 6(c) shows the copper-side fracture surface of the A0.2 sample, and Fig. 6(d) is the magnified image of Fig. 6(c). The presence of both Al-Zn eutectic and Al_2Cu at the surface can be confirmed by the XRD data in Fig. 7(a). In addition, the tearing ridge and cleavage surface can be observed in the microscopy image, which shows typical intergranular fracture features, and can be seen on the fracture surfaces. Figure 6(e) shows the fracture morphology of the B0.2 sample produced using ultrasound. The dark gray region in the figure is the diffusion layer that was mentioned in the EDS analysis in Sect. 3.2.2. Figure 6(f) is the magnified image of Fig. 6(e), which exhibits an intergranular fracture type. The lumpy $CuZn_5$ is distributed uniformly in the figure which the dendrite is not teared or deformed. Thus, the fracture may along the $CuZn_5$/Al-based solid solution surface. Figure 6(g) shows the fracture morphology of the B0.3 sample. Compared to that of the B0.2 sample, the interface of the B0.3 sample does not contain a large amount of $CuZn_5$, but $Al_{4.2}Cu_{3.2}Zn_{0.7}$ (identified by EDS and XRD) was found in the upper part of the picture.

4. Discussion

Based on the above results, most joints were broken near the copper side. That is, the interface layer near the copper side is the weak zone of the weld joint. This finding has also been illustrated in other research studies (Ref 22, 23). To analyze the influence of ultrasound assistance and zinc layers with different thicknesses on the quality of the welded joint, the copper side was specifically studied.

4.1 The Influence of Ultrasound Assistance on the Joint Interface

Figure 8(a) and (b) shows the SEM images of the Cu interface magnified in Fig. 4. The results of the EDS analysis at the locations marked in Fig. 8 are shown in Table 2. Figure 8(a) shows the Cu interface of sample A0.2, which was obtained without ultrasound. Some cracks, marked by arrows in the image, can be found in the reaction layer/filler metal interface, which may be detrimental to the reliability of the joint. Two interfacial layers with a measured thickness of approximately 3 μm can be found on the copper side. Table 2 shows that the upper layer is Al_2Cu and that the lower layer is a diffusion layer with a certain amount of Zn. Kuang et al. (Ref 24) found similar structures but did not explain this result. In fact, Al and Cu atoms have strong reactivity, and Al has a faster diffusion rate than that of Zn in the Cu matrix (Ref 25, 26), especially at high temperatures. As long as the atomic concentration reaches a certain level, Al_2Cu is the first IMC (Ref 27) produced in the interlayer. Figure 8(c) depicts the EDS scans of line 1 in Fig. 8(a), which show that the presence of less Zn and more Al and Cu elements resulted in the formation of the Al_2Cu and 1.2 μm diffusion layers. Integrated the fracture results and the IMC studies made above, the fracture of the joint starts at the interface layer of Al_2Cu and then extends to
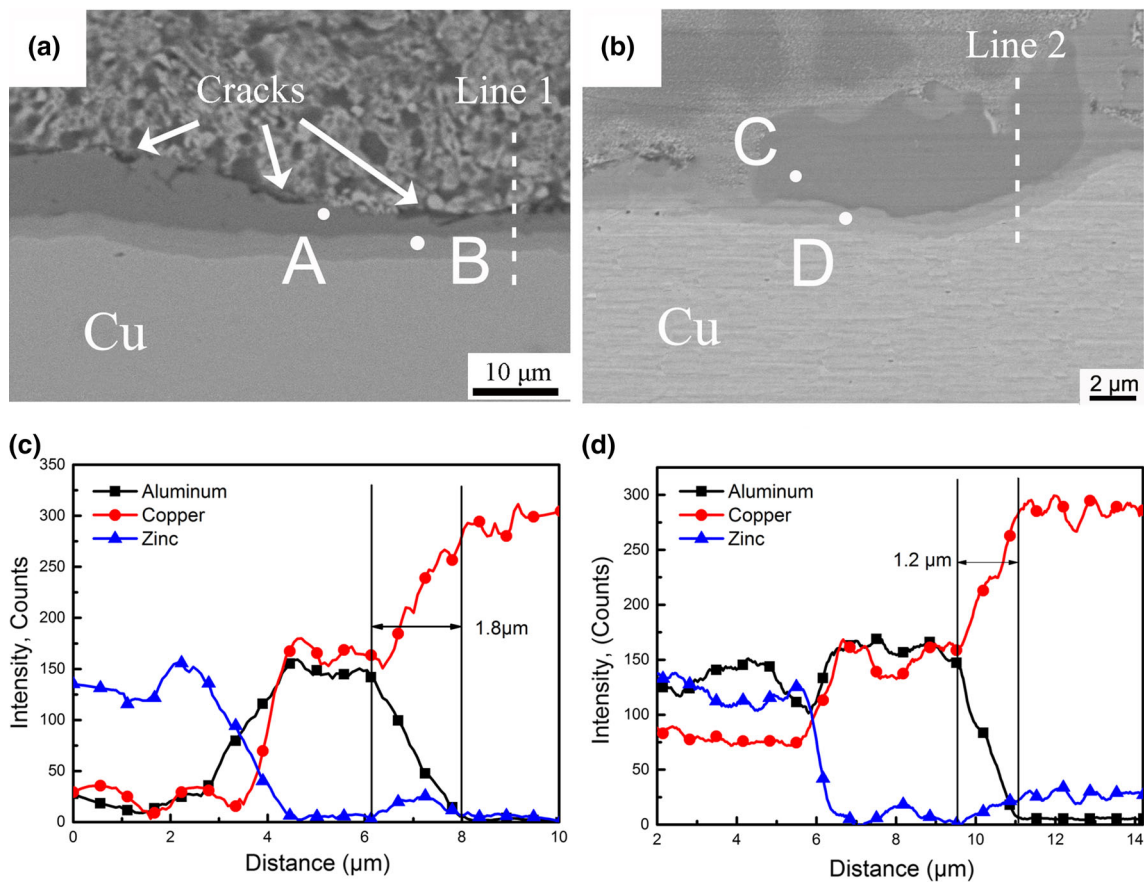
Fig. 8 SEM images near the Cu substrate of different samples. (a) A0.2 and (b) B0.2. (c) EDS line scan results of line 1 indicated in (a). (d) EDS line scan results of line 2 indicated in (b)

the middle until the fracture occurs. Due to the brittleness of Al_2Cu and the rapid propagation of cracks, its shear strength and elongation were low, as shown in Fig. 5(b).

Figure 8(b) shows the Cu interface of sample B0.2, which was prepared using ultrasound assistance. Compared to that of the joint welded without ultrasound assistance, the thickness of the Cu interfacial layer decreased to approximately 1.2 μm, as shown in Fig. 8(d). Based on the EDS results, the light gray layer at point B is a diffusion layer with a certain amount of dissolved Zn atoms, while the black block area at point A is Al_2Cu. Due to the cavitation effect of ultrasound, the elements in the interlayer are more uniformly distributed. As a result, the atomic concentration required to form lamellar Al_2Cu cannot be reached, and Al_2Cu can only be distributed in bulk at the copper interface. Consequently, this structure greatly improves the mechanical properties of the joint. Therefore, the reason that a large amount of $CuZn_5$ appears on the fracture surfaces of Fig. 6(e) and (f) can be explained, but Al_2Cu is hardly found. Notably, there is no tearing edge morphology in Fig. 6(f). Combining with Fig. 4(b), we can infer that the fracture location should be at the interface between $CnZn_5$ and Al-Zn eutectic, but not in the interior of Al-Zn eutectic.

To explain the formation process of the interlayer when ultrasound is applied, a schematic diagram of welding process is shown in Fig. 9. First, as the shoulder continues to approach,

Table 2 Element compositions and possible phase constitutions of the regions marked in Fig. 8

Samples	Regions	at.%	Phases
A0.2	A	69.67Al-30.33Cu	Al_2Cu
	B	41.70Al-48.28Cu-10.02Zn	Diffusion layer
B0.2	C	65.15Al-32.11Cu-2.74Zn	Al_2Cu
	D	31.32Al-66.58Cu-2.1Zn	Diffusion layer

once the temperature of the interlayer reaches zinc melting point of 419°C, the zinc layer begins to melt, and copper and zinc start dissolving into zinc, as shown in Fig. 9(a). Then, the shoulder moves directly above the zinc layer, the temperature continues to rise, and the diffusion intensifies. The near-copper side begins to react with zinc to form $CuZn_5$ and to react with the diffused aluminum to form a small amount of Al_2Cu due to the enrichment of copper atoms. Finally, because the reaction of Cu with Al gives priority to the formation of Al_2Cu, an Al_2Cu IMC layer with a certain thickness is formed in the enrichment zone on the copper side, as shown in Fig. 9(d). When ultrasound is applied, because of the cavitation effect, Al_2Cu is no longer distributed in layers near the copper side but as a small, fast shape at the interface, as shown in Fig. 9(c). The
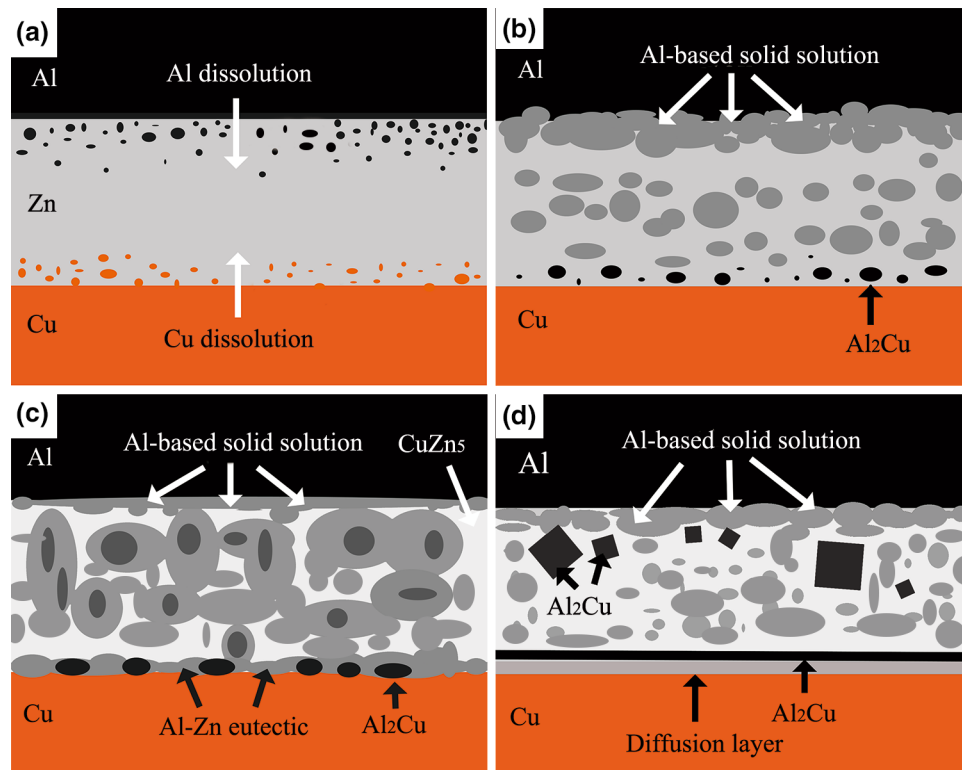
Fig. 9 Schematic diagram showing the formation mechanism of the interlayer structure during welding process. (a) Initial dissolution stage, (b) reaction stage, (c) final stage with ultrasound assistance, and (d) final stage without ultrasound assistance

intermediate layer is composed of refined Al-Zn eutectic and $CuZn_5$.

4.2 The Influence of Zn Thickness on the Joint Interface with Ultrasound Assistance

Increasing the filler zinc metal thickness to 0.3 mm, as shown in Fig. 10(a), leads to the formation of a thin serrate structure, and the thickness of the Cu interfacial layer increases to approximately 3.4 μm. Based on the EDS results shown in Table 3, the dark layers (marked "A") were estimated to be composed of an $Al_{4.2}Cu_{3.2}Zn_{0.7}$ phase, and the light gray layers (marked "B") are diffusion layers. According to the theory of ultrasound, when the clearance of the ultrasound action increases, its effect is weakened. As a result, this interface is not similar to that in Fig. 8(b). However, why was Al_2Cu not generated? This phenomenon may be related to the concentration of the liquid solder. Due to the increased thickness of the zinc foil (to 0.3 mm), the concentration of zinc in the liquid solder is increased, and there is more dissolved Al. Based on the phase diagram of Al-Cu-Zn ternary alloy (Ref 28), the formation energy of $Al_{4.2}Cu_{3.2}Zn_{0.7}$ is lower than that of $Al_{4.2}Cu_{3.2}Zn_{0.7}$ at the same temperature. In addition, the increased zinc content also promotes the formation of $Al_{4.2}Cu_{3.2}Zn_{0.7}$ at the Cu interface. According to the literature, $Al_{4.2}Cu_{3.2}Zn_{0.7}$ is a brittle IMC that has high rigidity and brittleness. In particular, the thickness of the IMC was more than 2 μm (Ref 29). As a result, when the joint is loaded, stress is easily concentrated in these areas, leading to joint failure (Ref 22). Therefore, the copper-side fracture interfaces of Fig. 6(g) and (h) distribute a large amount of $Al_{4.2}Cu_{3.2}Zn_{0.7}$ and show intergranular fracture. From the EDS line scan result shown in

Fig. 10(c), the diffusion layer decreased to 1 μm. This result indicated that the element diffusion was weakened.

Figure 10(b) shows the Cu interfaces of the B0.5 sample prepared with ultrasound assistance. The above analysis and EDS line scan results in Fig. 10(d) show that Al atoms could diffuse to the copper side because the zinc layer was not fully melted, and the copper-side interface could generate only $CuZn_5$ and a 5-μm-thick diffusion layer. Due to the theory of ultrasound, the cavitation effect must be reflected in the liquid phase, so the 0.5 mm zinc foil cannot be successfully connected under these conditions. This result also indicates that zinc can be fully diffused on the copper side due to the absence of other types of compounds. In other words, Al_2Cu and $Al_{4.2}Cu_{3.2}Zn_{0.7}$ can prevent the diffusion of Zn to the copper side.

5. Conclusion

In this paper, the microstructures and mechanical properties of Al/Zn/Cu friction stir welded joints prepared using ultrasound assistance are studied. In addition, the thickness of the Zn layer was varied to study the influence of the gap on the welding quality. The main conclusions are as follows:

(1) The use of ultrasound-assisted FSW can successfully yield welded joints without any holes or cracks.
(2) Joints prepared with ultrasound assistance and 0.2 mm Zn as the interlayer formed $CuZn_5$ and eutectic Al-Zn at the center of the welded joint and a discontinuous Al_2Cu layer near the copper side, suggesting that ultrasound caused a potential vibration and cavitation effect.
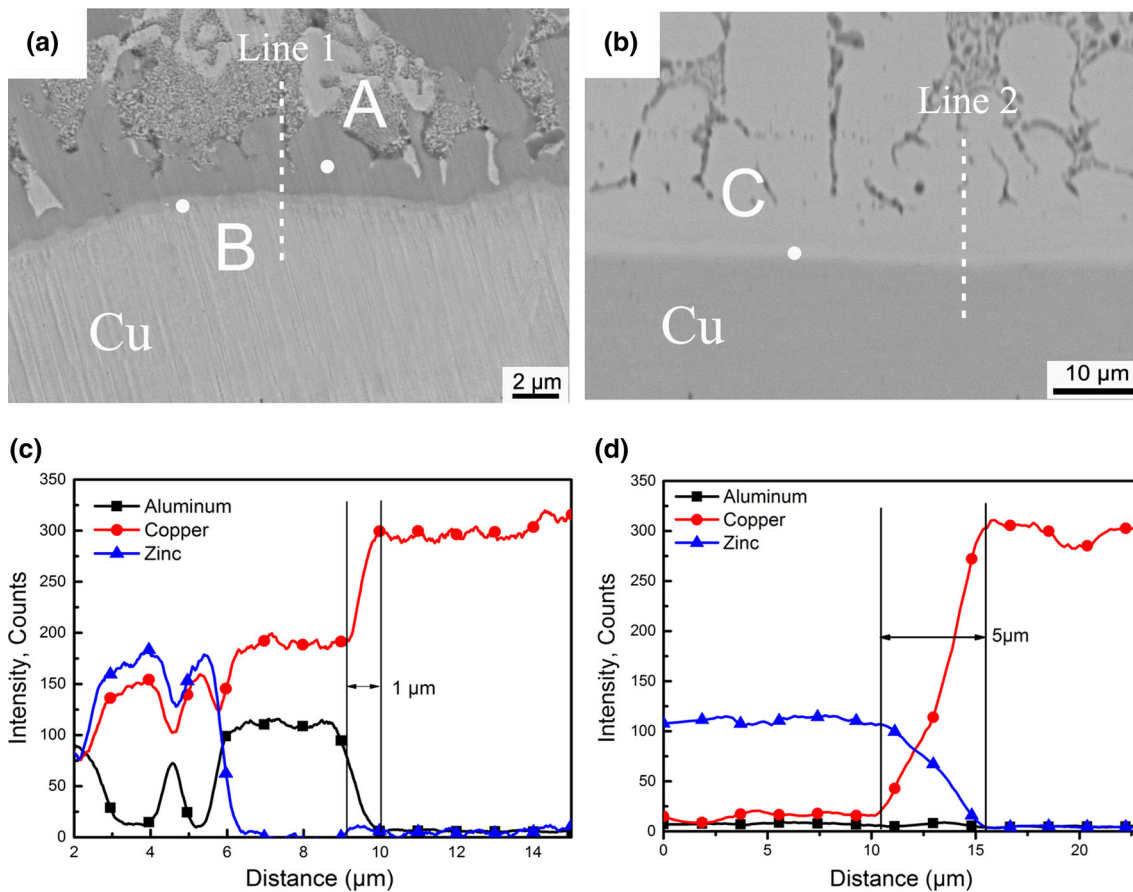
Fig. 10 SEM images near the Cu substrate of different samples. (a) B0.3, (b) B0.5. (c) EDS line scan results of line 1 indicated in (a); (d) EDS line scan results of line 2 indicated in (b)

Table 3 Element compositions and possible phase constitutions of the regions marked in Fig. 10

Samples	Regions	at.%	Phases
B0.3	A	48.48Al-41.55Cu-9.97Zn	$Al_{4.2}Cu_{3.2}Zn_{0.7}$
	B	24.32Al-55.01Cu-20.67Zn	Diffusion layer
B0.5	C	15.2Cu-84.8Zn	$CuZn_5$

However, when the joints were prepared without ultrasound, the interlayer structure formed a continuous Al_2Cu layer on the copper surface, which drastically reduced the resistance to crack propagation.

(3) With increasing zinc foil thickness, the effect of ultrasound gradually weakens. Al-to-Cu joints prepared with ultrasound assistance and 0.2 mm Zn as the interlayer had larger lap shear tensile strengths than those prepared using 0.3 mm or 0.5 mm Zn as the interlayer because joints made using a relatively thicker Zn interlayer produced IMCs of $Al_{4.2}Cu_{3.2}Zn_{0.7}$ or original zinc.

References

1. M. Felix Xavie Muthu and V. Jayabalan, Effect of Pin Profile and Process Parameters on Microstructure and Mechanical Properties of Friction Stir Welded Al-Cu Joints, *Trans. Nonferrous Metals Soc. China*, 2016, **26**(4), p 984–993

2. A.T. Kermanidis, P.I. Christodoulou, E. Hontzopoulos, G.N. Haidemenopoulo, H. Kamoutsi, and A.D. Zervaki, Mechanical Performance of Laser Spot-Welded Joints in Al-Al/Cu Solar Thermal Absorbers, *Mater. Des.*, 2018, **155**, p 148–160

3. Y.Y. Zhao, D. Li, and Y.S. Zhang, Effect of Welding Energy on Interface Zone of Al/Cu Ultrasonic Welded Joint, *Sci. Technol. Weld. Join.*, 2013, **18**(4), p 354–360

4. K. Paul and M.S. Jukka Martikainen, Trends in Joining Dissimilar Metals by Welding, *Mech. Mater.*, 2013, **440**, p 269–276

5. Q.Z. Zhang, W.B. Gong, and W. Liu, Microstructure and Mechanical Properties of Dissimilar Al-Cu Joints by Friction Stir Welding, *Trans. Nonferrous Metals Soc. China*, 2015, **25**(6), p 1779–1786

6. M. Simoncini and A. Forcellese, Effect of the Welding Parameters and Tool Configuration on Micro- and Macro-Mechanical Properties of Similar and Dissimilar FSWed Joints in AA5754 and AZ31 Thin Sheets, *Mater. Des.*, 2012, **41**, p 50–60

7. C.W. Tan, Z.G. Jiang, L.Q. Li, Y.B. Chen, and X.Y. Chen, Microstructural Evolution and Mechanical Properties of Dissimilar Al-Cu Joints Produced by Friction Stir Welding, *Mater. Des.*, 2013, **51**(5), p 466–473

8. I. Galvão, D. Verdera, D. Gesto, A. Loureiro, and D.M. Rodrigues, Influence of Aluminium Alloy Type on Dissimilar Friction Stir Lap Welding of Aluminium to Copper, *J. Mater. Process. Technol.*, 2013, **213**(11), p 1920–1928

9. J. Ouyang, E. Yarrapareddy, and R. Kovacevic, Microstructural Evolution in the Friction Stir Welded 6061 Aluminum Alloy (T6-temper condition) to Copper, *J. Mater. Process. Technol.*, 2006, **172**(1), p 110–122

10. E. Akca and A. Gursel, The Importance of Interlayers in Diffusion Welding-A Review, *Period Eng. Nat. Sci.*, 2015, **2**(3), p 12–16

11. J.P. Oliveira, B. Panton, Z. Zeng, C.M. Andrei, Y. Zhou, R.M. Miranda, and F.M. Braz Fernandes, Laser Joining of NiTi to Ti6Al4V Using a Niobium Interlayer, *Acta Mater.*, 2016, **105**(2), p 9–15

12. J.L. Murray, The Al-Zn (Aluminum-Zinc) System, *Bull. Alloy Phase Diagr*, 1983, **4**(1), p 55–73

13. P.E. Turchi, M. Sluiter, F.J. Pinski, D.D. Johnson, D.M. Nicholson, G.M. Stocks, and J.B. Staunton, First-Principles Study of Phase Stability in Cu-Zn Substitutional Alloys, *Phys. Rev. Lett.*, 1991, **67**(13), p 1779–1782

14. A. Elrefaey, M. Takahashi, and K. Ikeuchi, Preliminary Investigation of Friction Stir Welding Aluminium/Copper Lap Joints, *Weld. World*, 2005, **49**(3–4), p 93–101

15. G.F. Zhang, K. Zhang, L.J. Zhang, and J.X. Zhang, Approach to Disrupting Thick Intermetallic Compound Interfacial Layer in Friction Stir Brazing (FSB) of Al/Cu Plates, *Sci. Technol. Weld. Join.*, 2014, **19**(7), p 554–559

16. X. Chen, J. Yan, F. Gao, J. Wei, Z. Xu, and G. Fan, Interaction Behaviors at the Interface Between Liquid Al-Si and Solid Ti-6Al-4V in Ultrasonic-Assisted Brazing in Air, *Ultrason. Sonochem.*, 2013, **20**(1), p 144–154

17. Z. Ma, W. Zhao, J. Yan, and D. Li, Interfacial Reaction of Intermetallic Compounds of Ultrasonic-Assisted Brazed Joints Between Dissimilar Alloys of Ti$_6$Al$_4$V and Al$_4$Cu$_1$Mg, *Ultrason. Sonochem.*, 2011, **18**(5), p 1062–1067

18. S. Chen, Y. Zhou, J. Xue, R. Ni, Y. Guo, and J. Dong, High Rotation Speed Friction Stir Welding for 2014 Aluminum Alloy Thin Sheets, *J. Mater. Eng. Perform.*, 2017, **26**(3), p 1337–1345

19. J. Feng, S.B. Xue, and D. Wei, Reliability Studies of Cu/Al Joints Brazed with Zn-Al-Ce Filler Metals, *Mater. Des.*, 2012, **42**, p 156–163

20. C.Z. Xia, Q.H. Liang, and D.F. Chen, Investigation of Microstructure and Properties near the Interface of Copper/Aluminum Brazed Joint, *Kov. Mater.*, 2013, **51**(4), p 235–239

21. S. Chen, Z. Yang, J. Xue, R. Ni, G. Yue, and J. Dong, High Rotation Speed Friction Stir Welding for 2014 Aluminum Alloy Thin Sheets, *J. Mater. Eng. Perform.*, 2017, **26**, p 1–9

22. Y. Xiao, H. Ji, M. Li, and J. Kim, Ultrasound-Assisted Brazing of Cu/Al Dissimilar Metals Using a Zn-3Al Filler Metal, *Mater. Des.*, 2013, **52**(24), p 740–747

23. R. Balasundaram, V.K. Patel, S.D. Bhole, and D.L. Chen, Effect of Zinc Interlayer on Ultrasonic Spot Welded Aluminum-to-Copper Joints, *Mater. Sci. Eng. A*, 2014, **607**, p 277–286

24. B. Kuang, Y. Shen, W. Chen, X. Yao, H. Xu, and J. Gao, The Dissimilar Friction Stir Lap Welding of 1A99 Al to Pure Cu Using Zn as Filler Metal with "Pinless" Tool Configuration, *Mater. Des.*, 2015, **68**, p 54–62

25. W.B. Lee, K.S. Bang, and S.B. Jung, Effects of Intermetallic Compound on the Electrical and Mechanical Properties of Friction Welded Cu/Al Bimetallic Joints During Annealing, *J. Alloys Compd.*, 2005, **390**(1–2), p 219

26. Z. Wei, L. Liu, B. Li, Q. Song, and P. Wu, Structural, Elastic, and Electronic Properties of Al-Cu Intermetallics from First-Principles Calculations, *J. Electron. Mater.*, 2009, **38**(2), p 356–364

27. P. Xue, B.L. Xiao, D.R. Ni, and Z.Y. Ma, Enhanced Mechanical Properties of Friction Stir Welded Dissimilar Al-Cu Joint by Intermetallic Compounds, *Mater. Sci. Eng. A*, 2010, **527**(21), p 5723–5727

28. H. Liang and Y.A. Chang, A Thermodynamic Description for the Al-Cu-Zn System, *J. Phase Equilib. Diffus.*, 1998, **19**(1), p 25–37

29. M. Braunovic and N. Alexandrov, Intermetallic Compounds at Aluminum-to-Copper Electrical Interfaces: Effect of Temperature and Electric Current, *IEEE Trans. Compon. Pack. A*, 1994, **17**(1), p 78–85